Symmetric BEM Formulation for the M/EEG Forward Problem

Geoffray Adde, Maureen Clerc, Olivier Faugeras, Renaud Keriven, Jan Kybic, and Théodore Papadopoulo

Odyssée Laboratory – ENPC - ENS Ulm - INRIA – France
Maureen.Clerc@cermics.enpc.fr, kybic@ieee.org,
home page: http://www-sop.inria.fr/odyssee

Abstract. The forward M/EEG problem consists in simulating the electric potential and the magnetic field produced outside the head by currents in the brain related to neural activity. All previously proposed solutions using the Boundary Element Method (BEM) were based on a double-layer integral formulation. We have developed an alternative symmetric BEM formulation, achieving a significantly higher accuracy for sources close to tissue interfaces, namely in the cortex. Numerical experiments using a spherical semi-realistic multilayer head model with a known analytical solution are presented, showing that the new BEM performs better than the formulations used in our earlier comparisons, and in most cases outperforms the Finite Element Method (FEM) as far as accuracy is concerned, thus making the BEM a viable choice.

1 Introduction

The so-called *forward problem* of electro-encephalography (EEG) addresses the calculation of the electric potential V on the scalp for a known configuration of sources, provided that the physical properties of the head tissues (conductivities) are also known. Note that the same forward model as for the EEG [**?**] can be used for the magneto-encephalography (MEG) [1, 2] as well, since the magnetic field can be calculated from the potential V by simple integration [3], see also Section 3.3. An accurate solution of the forward problem is a necessary prerequisite for solving the *inverse problem*, and is extremely important to take maximum benefit from the EEG and the costly MEG machines, which have the advantages of noninvasiveness and excellent time resolution but presently lag seriously behind alternative technologies such as fMRI in terms of spatial resolution.

The potential V is related to the primary current sources $\mathbf{J}^{\mathrm{p}}$ through the generalized Poisson equation

$$\nabla \cdot \big(\sigma \nabla V\big) = f = \nabla \cdot \mathbf{J}^{\mathrm{p}} \quad \text{in } \mathbb{R}^3 \tag{1}$$

which derives directly from the Maxwell equations in the quasi-static (low frequency) regime.

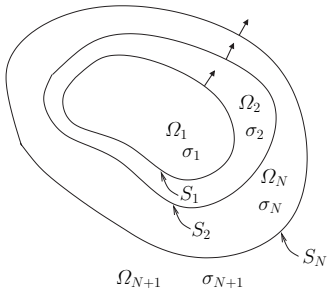

Fig. 1. The head is modeled as a set of nested regions $\Omega_1, \ldots, \Omega_{N+1}$ with constant conductivities $\sigma_1, \ldots, \sigma_{N+1}$, separated by interfaces $S_1, \ldots, S_N$. Arrows indicate the outward normal $\mathbf{n}$.

We shall concentrate here on a head model consisting of regions with homogeneous conductivities (Fig. 1), the conductivity of air σ_{N+1} being zero. Because of the piecewise-constant conductivity assumption, the problem (1) can be decomposed as

$$\sigma_i \Delta V = f \quad \text{in } \Omega_i, \text{ for all } i = 1, \ldots, N+1 \tag{2}$$

$$\big[V\big]_j = \big[\sigma \partial_{\mathbf{n}} V\big]_j = 0 \quad \text{on } S_j, \text{ for all } j = 1, \ldots, N \tag{3}$$

where $\partial_{\mathbf{n}} V = \frac{\partial V}{\partial \mathbf{n}}$ is the normal derivative on S_j and where $[\cdot]_j$ denotes the jump across an oriented interface S_j. For example for $\mathbf{r} \in S_j$,

$$\big[V\big]_j(\mathbf{r}) = \lim_{\alpha \to 0^+} \left(V(\mathbf{r} - \alpha\, \mathbf{n}) - V(\mathbf{r} + \alpha\, \mathbf{n})\right) \stackrel{\text{def}}{=} V^-(\mathbf{r}) - V^+(\mathbf{r}) \ .$$

The Boundary Element Method (BEM) [4] is based on integral equations involving unknowns on the interfaces, whereas the FDM (finite difference method) or FEM (finite element method) consider the entire volume. Thus the BEM greatly reduces the number of unknowns, and has the advantage of requiring only surface meshes instead of volume meshes.

A disadvantage often reported for the BEM and much improved by the present approach, is the drop of precision when the distance d of the source to one of the surfaces becomes comparable to the size h of the triangles in the mesh [5–7],[8]. This is a problem, because for physiological reasons, one mainly considers the primary currents to lie in the cortex, a layer only a few millimeters thick. Therefore, to obtain a satisfactory precision, the surface of the cortex must be discretized extremely finely.

In Section 2, we recall the Representation Theorem which allows to consider unknowns on a surface, instead of volume quantities. We establish the classical BEM formulation using a double-layer potential in Section 3.1. This formulation, introduced by Geselowitz [9] in 1967, has been the base of all previous BEM implementations. In Section 3.2, we present the new method, which involves an

additional unknown $\partial_{\mathbf{n}} V$, and which has the advantage of leading to a symmetric system matrix. Finally, we present numerical results in Section 4, showing mainly that the new symmetric integral formulation performs much better than the classical BEM in terms of precision.

2 Integral representations

The fundamental Representation Theorem of potential theory, which we recall below, shows that a harmonic function[1] u is determined everywhere in $\mathbb{R}^3$ by its jump and the jump of its derivative across a boundary $\partial\Omega$, whether $\partial\Omega$ is composed of a single surface, or of two surfaces as on the left of Fig. 2 – the latter case being proved in [10].

We start by defining the four integral operators $\mathcal{S}$, $\mathcal{D}$, $\mathcal{D}^*$ and $\mathcal{N}$ involved in the Representation Theorem. Given the Green function $G(\mathbf{r}) = \frac{1}{4\pi\|\mathbf{r}\|}$, which satisfies

$$-\Delta G = \delta_0$$

where δ_0 is a Dirac mass centered at position 0, the *double-layer* and *single-layer* integral operators are defined by

$$\big(\mathcal{D}f\big)(\mathbf{r}) = \int_{\partial\Omega} \partial_{\mathbf{n}'} G(\mathbf{r}-\mathbf{r}') f(\mathbf{r}')\,\mathrm{d}s(\mathbf{r}') \;, \tag{4}$$

$$\big(\mathcal{S}f\big)(\mathbf{r}) = \int_{\partial\Omega} G(\mathbf{r}-\mathbf{r}') f(\mathbf{r}')\,\mathrm{d}s(\mathbf{r}') \;. \tag{5}$$

where $\mathbf{r} \in \mathbb{R}^3$ and $\mathbf{n}'$ denotes the outward normal vector at $\mathbf{r}' \in \partial\Omega$. The double-layer potential $\big(\mathcal{D}f\big)$ is discontinuous across $\partial\Omega$ whereas its normal derivative is continuous:

$$[\mathcal{D}f]_{\partial\Omega} = -f \;, \qquad \left[\tfrac{\partial \mathcal{D}f}{\partial \mathbf{n}}\right]_{\partial\Omega} = 0 \;.$$

The single-layer potential $\big(\mathcal{S}f\big)$ defined by (5) has the opposite properties:

$$[\mathcal{S}f]_{\partial\Omega} = 0 \;, \qquad \left[\tfrac{\partial \mathcal{S}f}{\partial \mathbf{n}}\right]_{\partial\Omega} = f \;.$$

Both the double-layer and the single-layer potentials are harmonic everywhere except on $\partial\Omega$. We next define two integral operators, obtained through differentiation of (4) and (5) in a direction $\mathbf{n}$:

$$\big(\mathcal{N}f\big)(\mathbf{r}) = \int_{\partial\Omega} \partial^2_{\mathbf{n},\mathbf{n}'} G(\mathbf{r}-\mathbf{r}') f(\mathbf{r}')\,\mathrm{d}s(\mathbf{r}')$$

$$\big(\mathcal{D}^*f\big)(\mathbf{r}) = \int_{\partial\Omega} \partial_{\mathbf{n}} G(\mathbf{r}-\mathbf{r}') f(\mathbf{r}')\,\mathrm{d}s(\mathbf{r}') \;.$$

Finally, we state the Representation Theorem:

[1] A function u is harmonic if its Laplacian Δu vanishes.

Theorem 1 (Representation Theorem). *Let $\Omega \subseteq \mathbb{R}^3$ be a bounded open set with a regular boundary $\partial\Omega$. Let $u : (\mathbb{R}^3 \backslash \partial\Omega) \to \mathbb{R}$ be a harmonic function ($\Delta u = 0$ in $\mathbb{R}^3 \backslash \partial\Omega$), decreasing at least as $\|\mathbf{r}\|^{-1}$ at infinity[2], and let $p(\mathbf{r}) \stackrel{def}{=} \partial_{\mathbf{n}} u(\mathbf{r})$. Then*

$$\begin{array}{rcccl} -p = & +\mathcal{N}\,[u] & -\mathcal{D}^*\,[p] & \text{in } \mathbb{R}^3 \backslash \partial\Omega \\ u = & -\mathcal{D}\,[u] & +\mathcal{S}\,[p] & \\ -p^{\pm} = & +\mathcal{N}\,[u] & +\left(\pm\frac{\mathcal{I}}{2} - \mathcal{D}^*\right)[p] & \text{on } \partial\Omega \\ u^{\pm} = & \left(\mp\frac{\mathcal{I}}{2} - \mathcal{D}\right)[u] & +\mathcal{S}\,[p] & \end{array}$$

where $\mathcal{I}$ denotes the identity operator.

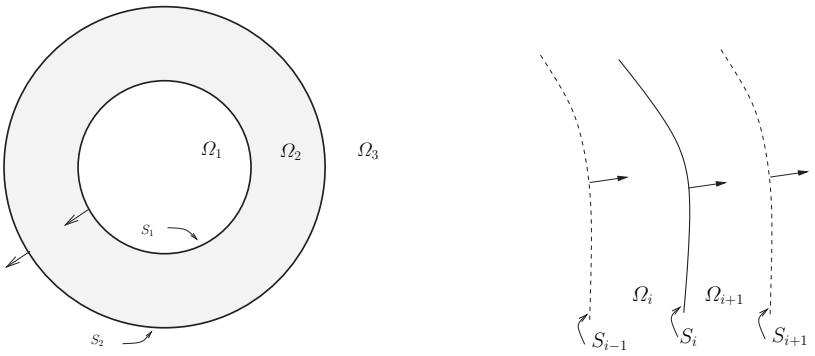

Fig. 2. Left: two-dimensional slice through a volume Ω_2 with a hollow ball topology. Arrows denote the normal orientation. **Right:** detail of a nested volume model. Normal vectors are oriented globally outward, as shown. However, when considering for example the surface S_i as the boundary of Ω_{i+1}, the displayed orientation becomes locally inward.

3 Integral Formulations for M/EEG

3.1 Double-layer Potential

The Boundary Element Method classically used for the M/EEG reconstruction can be expressed using the double-layer potential. Let us examine the case of a conductor Ω with homogeneous conductivity σ_0, placed inside a non-conductive medium. The potential V which satisfies (1), with a source f supported inside Ω, is decomposed as $\sigma V = V_0 + u$, where $\sigma = \sigma_0$ inside Ω, $\sigma = 0$ outside Ω, and V_0 is the homogeneous domain solution:

$$\sigma_0 \Delta V_0 = f \ .$$

[2] This is called the "radiation condition" $\mathscr{H}$. See [4] or [10] for details.

Considering the Green function G introduced in Section 2, the homogeneous domain solution is simply $V_0 = -(f \star G)/\sigma_0$.

By definition, the function u is harmonic inside and outside Ω, and also satisfies $[\partial_{\mathbf{n}} u] = 0$ across the boundary $\partial\Omega$. It can therefore be represented as a double-layer potential $\mathcal{D}[u]$. The Representation Theorem shows that the exterior limit of u on $\partial\Omega$ is

$$u^+ = -\frac{[u]}{2} - \mathcal{D}[u] \ ,$$

and since $u^+ = -V_0$ and $[u] = \sigma_0 V$, we obtain the integral relation on $\partial\Omega$:

$$V_0 = \frac{\sigma_0 V}{2} + \sigma_0 \mathcal{D} V \ .$$

The extension to multiple interfaces (Fig. 1) yields

$$(V_0)_{S_j} = \tfrac{\sigma_{j-1}+\sigma_j}{2} V_{S_j} + \sum_i (\sigma_{i-1}-\sigma_i) \mathcal{D}_{ji} V_{S_i}$$

where V_{S_i} denotes the potential considered on interface S_i and $\mathcal{D}_{ji}$ is the integral operator which couples interfaces S_i and S_j. Writing down explicitly the operator $\mathcal{D}_{ji}$, we obtain the well-known relation between V_0 and V: for $\mathbf{r} \in S_j$,

$$V_0(\mathbf{r}) = \tfrac{\sigma_{j-1}+\sigma_j}{2} V(\mathbf{r}) + \sum_i (\sigma_{i-1} - \sigma_i) \int_{S_i} \partial_{\mathbf{n}'} G(\mathbf{r} - \mathbf{r}') \, V(\mathbf{r}') \, \mathrm{d}s(\mathbf{r}') \ .$$

3.2 Symmetric Method

The symmetric approach, based on the theory of Nédélec [4] and related to algorithms in [11, 12], has, to the best of our knowledge, never been applied to the E/MEG problem. We consider the nested volume case depicted in Fig. 1, and decompose the source as $f = f_1 + \cdots + f_N$ such that $supp\, f_i \subset \Omega_i$. For a given $i \in \{1, \ldots, N\}$ (Fig. 2, right), we consider the function

$$u_{\Omega_i} = \begin{cases} V - v_{\Omega_i}/\sigma_i & \text{in } \Omega_i \\ -v_{\Omega_i}/\sigma_i & \text{in } \mathbb{R}^3 \backslash \overline{\Omega}_i, \end{cases} \tag{6}$$

where $v_{\Omega_i} = -f_i \star G$ is the homogeneous space solution of $\Delta v_{\Omega_i} = f_i$. Note that u_{Ω_i} is harmonic in $\mathbb{R}^3 \backslash \partial\Omega_i$.

The Representation Theorem provides the internal limit of u_{Ω_i} on S_i:

$$\big(u_{\Omega_i}\big)^-_{S_i} = \frac{\big[u_{\Omega_i}\big]_{\partial\Omega_i}}{2} - \mathcal{D}_{\partial\Omega_i}\big[u_{\Omega_i}\big]_{\partial\Omega_i} + \mathcal{S}_{\partial\Omega_i}\big[\partial_{\mathbf{n}} u_{\Omega_i}\big]_{\partial\Omega_i} \ .$$

Defining $p_{S_i} = \sigma_i [\partial_{\mathbf{n}} u_{\Omega_i}]_{S_i} = \sigma_i (\partial_{\mathbf{n}} V)^-_{S_i}$ and breaking down the integral operators on $\partial\Omega_i = S_{i-1} \cup S_i$ yields

$$\begin{aligned} \big(u_{\Omega_i}\big)^-_{S_i} &= \big(V - v_{\Omega_i}/\sigma_i\big)^-_{S_i} \\ &= \frac{V_{S_i}}{2} + \mathcal{D}_{i,i-1} V_{S_{i-1}} - \mathcal{D}_{ii} V_{S_i} - \sigma_i^{-1} \mathcal{S}_{i,i-1} p_{S_{i-1}} + \sigma_i^{-1} \mathcal{S}_{ii} p_{S_i} \ . \end{aligned} \tag{7}$$

We next consider the function $u_{\Omega_{i+1}}$ defined as in (6), and again apply the Representation Theorem to calculate its external limit on S_i:

$$\big(u_{\Omega_{i+1}}\big)^+_{S_i} = -\frac{\big[u_{\Omega_{i+1}}\big]_{\partial\Omega_{i+1}}}{2} - \mathcal{D}_{\partial\Omega_{i+1}}\big[u_{\Omega_{i+1}}\big]_{\partial\Omega_{i+1}} + \mathcal{S}_{\partial\Omega_{i+1}}\big[\partial_{\mathbf{n}} u_{\Omega_{i+1}}\big]_{\partial\Omega_{i+1}} \ ,$$

and breaking down once again the integral operators,

$$\begin{aligned}\big(u_{\Omega_{i+1}}\big)^+_{S_i} &= \big(V - v_{\Omega_{i+1}}/\sigma_{i+1}\big)^+_{S_i} \\ &= \frac{V_{S_i}}{2} + \mathcal{D}_{ii}V_{S_i} - \mathcal{D}_{i,i+1}V_{S_{i+1}} - \sigma_{i+1}^{-1}\mathcal{S}_{ii}p_{S_i} + \sigma_{i+1}^{-1}\mathcal{S}_{i,i+1}p_{S_{i+1}} \ .\end{aligned} \tag{8}$$

Finally, subtracting (8) from (7) gives

$$\begin{aligned}&\sigma_{i+1}^{-1}(v_{\Omega_{i+1}})_{S_i} - \sigma_i^{-1}(v_{\Omega_i})_{S_i} = \mathcal{D}_{i,i-1}V_{S_{i-1}} - 2\mathcal{D}_{ii}V_{S_i} + \mathcal{D}_{i,i+1}V_{S_{i+1}} \\ &- \sigma_i^{-1}\mathcal{S}_{i,i-1}p_{S_{i-1}} + (\sigma_i^{-1} + \sigma_{i+1}^{-1})\mathcal{S}_{ii}p_{S_i} - \sigma_{i+1}^{-1}\mathcal{S}_{i,i+1}p_{S_{i+1}} \quad \text{for } i = 1, \dots, N.\end{aligned} \tag{9}$$

Using the same approach, we evaluate the quantities $\big(\sigma_i\partial_{\mathbf{n}}u_{\Omega_i}\big)^-_{S_i} = \big(p - \partial_{\mathbf{n}}v_{\Omega_i}\big)^-_{S_i}$ and $\big(\sigma_{i+1}\partial_{\mathbf{n}}u_{\Omega_{i+1}}\big)^+_{S_i} = \big(p - \partial_{\mathbf{n}}v_{\Omega_{i+1}}\big)^+_{S_i}$ with the Representation Theorem, subtract the resulting expressions and obtain

$$\begin{aligned}(\partial_{\mathbf{n}}v_{\Omega_{i+1}})_{S_i} - (\partial_{\mathbf{n}}v_{\Omega_i})_{S_i} &= \sigma_i\mathcal{N}_{i,i-1}V_{S_{i-1}} - (\sigma_i + \sigma_{i+1})\mathcal{N}_{ii}V_{S_i} + \sigma_{i+1}\mathcal{N}_{i,i+1}V_{S_{i+1}} \\ &- \mathcal{D}^*_{i,i-1}p_{S_{i-1}} + 2\mathcal{D}^*_{ii}p_{S_i} - \mathcal{D}^*_{i,i+1}p_{S_{i+1}} \quad \text{for } i = 1, \dots, N\end{aligned} \tag{10}$$

Observe that each surface S_i only interacts with its two neighbors S_{i-1} and S_{i+1}. This leads to an operator matrix which is not only symmetric, but also block-diagonal. The assumption $\sigma_{N+1} = 0$ has the consequence of effectively chopping off the last line and column of the matrix – see the explicit system detailed in (11).

3.3 Magnetic Field Computation

It is well-known that the magnetic field $\mathbf{B}$ is entirely determined from the knowledge of V on the interfaces [3]. More precisely

$$\mathbf{B}(\mathbf{r}) = \mathbf{B}_0(\mathbf{r}) + \tfrac{\mu_0}{4\pi}\sum_i (\sigma_i - \sigma_{i+1}) \int_{S_i} V(\mathbf{r}')\,\mathbf{n}(\mathbf{r}') \times \frac{\mathbf{r} - \mathbf{r}'}{\|\mathbf{r} - \mathbf{r}'\|}\,\mathrm{d}s(\mathbf{r}') \ ,$$

where $\mathbf{B}_0$ represents the magnetic field due to primary currents in a homogeneous medium

$$\mathbf{B}_0(\mathbf{r}) = \frac{\mu_0}{4\pi}\int_{\mathbb{R}^3} \mathbf{J}^{\mathrm{p}}(\mathbf{r}') \times \frac{\mathbf{r} - \mathbf{r}'}{\|\mathbf{r} - \mathbf{r}'\|}\,\mathrm{d}V(\mathbf{r}') \ .$$

4 Discretization and numerical experiments

4.1 Galerkin approach

The surfaces are represented by triangular meshes, the potential V is approximated using P1 (piecewise-linear) basis functions as $V_{S_k}(\mathbf{r}) = \sum_i x_i^{(k)} \phi_i^{(k)}(\mathbf{r})$, while p is represented in the space of P0 (piecewise-constant) basis functions, $p_{S_k}(\mathbf{r}) = \sum_i y_i^{(k)} \psi_i^{(k)}(\mathbf{r})$. This choice guarantees the asymptotic equivalence between two sources of error: the approximation of smooth surfaces by triangulated meshes, and the approximation of V and p. The equations (9),(10) are discretized using the Galerkin method. The equation (9) corresponding to the potential V is integrated against P0 test functions, and the equation (10) corresponding to the flow p is integrated against P1 test functions. This again has the consequence of balancing the approximation errors. We obtain a symmetric block-diagonal matrix system, given here in more detail:

$$
\begin{bmatrix}
(\sigma_1+\sigma_2)\mathsf{N}_{11} & -2\mathsf{D}_{11}^* & -\sigma_2\mathsf{N}_{12} & \mathsf{D}_{12}^* & & & \\
-2\mathsf{D}_{11} & (\sigma_1^{-1}+\sigma_2^{-1})\mathsf{S}_{11} & \mathsf{D}_{12} & -\sigma_2^{-1}\mathsf{S}_{12} & & & \\
-\sigma_2\mathsf{N}_{21} & \mathsf{D}_{21}^* & (\sigma_2+\sigma_3)\mathsf{N}_{22} & -2\mathsf{D}_{22}^* & -\sigma_3\mathsf{N}_{23} & \mathsf{D}_{23}^* & \\
\mathsf{D}_{21} & -\sigma_2^{-1}\mathsf{S}_{21} & -2\mathsf{D}_{22} & (\sigma_2^{-1}+\sigma_3^{-1})\mathsf{S}_{22} & \mathsf{D}_{23} & -\sigma_3^{-1}\mathsf{S}_{23} & \\
 & & -\sigma_3\mathsf{N}_{32} & \mathsf{D}_{32}^* & (\sigma_3+\sigma_4)\mathsf{N}_{33} & -2\mathsf{D}_{33}^* & \dots \\
 & & \mathsf{D}_{32} & -\sigma_3^{-1}\mathsf{S}_{32} & -2\mathsf{D}_{33} & (\sigma_3^{-1}+\sigma_4^{-1})\mathsf{S}_{33} & \dots \\
 & & & & \vdots & \vdots & \ddots \\
\end{bmatrix}
\begin{bmatrix}
\ddots & \vdots & \vdots & \\
\dots & (\sigma_{N-1}+\sigma_N)\mathsf{N}_{N-1,N-1} & -2\mathsf{D}_{N-1,N-1}^* & -\sigma_N\mathsf{N}_{N-1,N} \\
\dots & -2\mathsf{D}_{N-1,N-1} & (\sigma_{N-1}^{-1}+\sigma_N^{-1})\mathsf{S}_{N-1,N-1} & \mathsf{D}_{N-1,N} \\
 & -\sigma_N\mathsf{N}_{N,N-1} & \mathsf{D}_{N,N-1}^* & \sigma_N\mathsf{N}_{N,N}
\end{bmatrix}
\begin{bmatrix}
\mathbf{x}_1 \\ \mathbf{y}_1 \\ \mathbf{x}_2 \\ \mathbf{y}_2 \\ \mathbf{x}_3 \\ \mathbf{y}_3 \\ \vdots
\end{bmatrix}
=
\begin{bmatrix}
\mathbf{b}_1 \\ \mathbf{c}_1 \\ \mathbf{b}_2 \\ \mathbf{c}_2 \\ \mathbf{b}_3 \\ \mathbf{c}_3 \\ \vdots
\end{bmatrix}
\tag{11}
$$

The indices k, l of the operators refer to interfaces S_k and S_l. Each block is a submatrix, representing the interactions between all test functions supported on a given pair of surfaces. Denoting $\psi_i^{(k)}$ the P0 function associated to element i on surface S_k, and $\phi_j^{(l)}$ the P1 function associated to element j on surface S_l, we have

$$
\begin{aligned}
&\big(\mathsf{N}_{kl}\big)_{ij} = \big\langle \mathcal{N}_{kl}\phi_j^{(l)}, \phi_i^{(k)} \big\rangle && \big(\mathsf{S}_{kl}\big)_{ij} = \big\langle \mathcal{S}_{kl}\psi_j^{(l)}, \psi_i^{(k)} \big\rangle \\
&\big(\mathsf{D}_{kl}\big)_{ij} = \big(\mathsf{D}_{lk}^*\big)_{ji} = \big\langle \mathcal{D}_{kl}\phi_j^{(l)}, \psi_i^{(k)} \big\rangle \\
&\big(\mathbf{b}_k\big)_i = \Big\langle \partial_{\mathbf{n}} v_k - \partial_{\mathbf{n}} v_{k+1}, \phi_i^{(k)} \Big\rangle && \big(\mathbf{c}_k\big)_i = \Big\langle \sigma_{k+1}^{-1} v_{\Omega_{k+1}} - \sigma_k^{-1} v_{\Omega_k}, \psi_i^{(k)} \Big\rangle \\
&\big(\mathbf{x}_k\big)_i = x_i^{(k)} && \big(\mathbf{y}_k\big)_i = y_i^{(k)}
\end{aligned}
$$

The potential V being only defined up to a constant, the above system has an indeterminacy, which is lifted by deflating the last block $\sigma_N \mathsf{N}_{N,N}$ [13–15].

4.2 Experiments

We compare the above-described symmetric BEM with the classical (double-layer) BEM for several discretization choices, and with the Finite Element Method (FEM).

The tests are performed on a simplified head model for which an analytical solution exists [16–18]. It consists of three spherical surfaces with radii 0.87, 0.92, and 1.0, delimiting volumes with conductivities 1.0, 0.0125, 1.0, and 0.0, from inside towards outside. The sources are unitary current dipoles oriented as $[1\ 0\ 1]/\sqrt{2}$ and placed at distances from the center equal to $49\%, 78\%, 88\%, 93\%,$ or 97% of the radius of the innermost sphere. The spherical surfaces are triangulated with progressively finer meshes of $42, 162, 642,$ and 2562 vertices. The relative error measure is $\|V - V_{\text{anal}}\|_{\ell_2} / \|V_{\text{anal}}\|_{\ell_2}$, where the ℓ_2 norm is integrated over the entire outer sphere (representing the scalp).

The first set of experiments (Fig. 3) shows how the relative error increases when the current dipole source approaches the surface of discontinuity. We observe that the symmetric approach behaves better than the classical BEM.

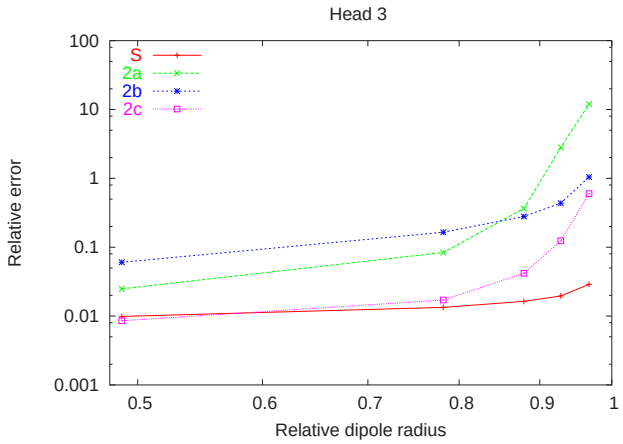

Fig. 3. The relative ℓ_2 error versus the relative dipole position for meshes with 642 vertices per sphere. The label 2 refers to the double-layer potential formulation, a,b,c are respectively the P0-collocation[18], and P0-P0 and P1-P1 Galerkin discretizations. The label S refers to the symmetric formulation.

The second set of experiments shows the evolution of the relative error as a function of the ratio of the conductivity of the middle layer of our three-sphere model with respect to the other two layers. Here again we observe a

better behavior of the symmetric method compared to the classical double-layer BEM, the accuracy of which is generally improved by using an Isolated Problem Approach [19].

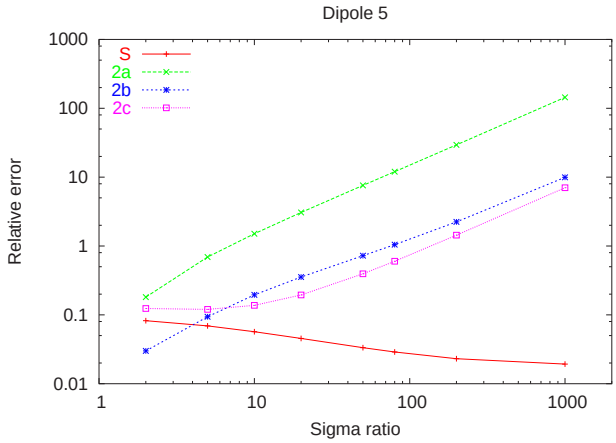

Fig. 4. The relative error versus the ratio of conductivities between neighboring layers, for the dipole at 97% of the inner sphere radius and a mesh of 3×642 vertices. (Labels are the same as in Fig. 3.)

Finally, we compare the new symmetric BEM, so far the best BEM known to us, with the FEM which we used in a previous comparison [20]. The accuracy results are in Table 1. We observe that unless the dipole source is extremely close to the surface, the new BEM method provides better precision than the FEM. Equivalent meshes were used in both cases, coinciding on the triangles for all surfaces.

We also compare the time requirements for BEM and FEM. Table 2 details the time needed to assemble the BEM system matrix and to solve it using either a direct or an iterative method, as compared with the time required for the FEM.

5 Conclusions

We have presented a symmetric BEM formulation, which is new to the field of M/EEG. We have shown that it outperforms the previously used formulations and we have found that unlike these [20], the new BEM is in most cases more accurate than the FEM as well.

There are various ways of accelerating the BEM implementation and bringing it on-par with the FEM, among which iterative solvers [5, 6, 21], the fast multipole method (FMM) [8], precorrected-FFT [22, 23] or SVD-based methods.

Table 1. The relative ℓ_2 error of the symmetric BEM and FEM, for all three head models and 5 dipole positions. Values marked in bold show the more accurate of the two methods for a particular head/dipole combination.

Symmetric BEM

Dipole pos.	49%	78%	88%	93%	97%
Head 1	**0.1536**	**0.1658**	**0.1900**	0.2273	0.3172
Head 2	**0.0387**	**0.0469**	**0.0539**	**0.0661**	**0.0892**
Head 3	**0.0099**	**0.0134**	**0.0164**	**0.0196**	**0.0289**

FEM

Dipole pos.	49%	78%	88%	93%	97%
Head 1	0.2468	0.2107	0.2852	**0.2250**	**0.1398**
Head 2	0.0784	0.1738	0.0660	0.1415	0.1172
Head 3	0.0142	0.0323	0.0194	0.0608	0.0791

Table 2. Typical execution times for the symmetric BEM and for the FEM for varying model sizes.

Triangles per sphere		80	320	1280	5120
BEM	Unknowns	286	1126	4486	17926
	Assembly	0.42 s	7.28 s	147 s	72 min
	Direct solution	0.03 s	1.55 s	93.21 s	$\approx$ 100 min
	Iterative solution[a]	$\approx$ 0.01 s	$\approx$ 0.3 s	$\approx$ 6 s	$\approx$ 5 min
FEM	Unknowns	156	807	4881	32053
	Iterative solution	0.1 s	0.3 s	2.8 s	31.9 s

[a] A preconditioned GMRES method was used. The reported times should be taken as a coarse indication only, as the number of iteration and thus the total elapsed time varies enormously with the precision demanded and the source configuration.

Future work includes better understanding of the accuracy improvements and consequential development of the symmetric method, as well as its application in the inverse problem context.

Acknowledgements

We are grateful to Toufic Abboud, Alain Dervieux and Guillaume Sylvand for fruitful discussions.

References

1. Jukka Sarvas, "Basic mathematical and electromagnetic concepts of the biomagnetic inverse problem," *Phys. Med. Biol.*, vol. 32, no. 1, pp. 11–22, 1987.
2. Matti Hämäläinen, Riitta Hari, Risto J. IImoniemi, Jukka Knuutila, and Olli V. Lounasmaa, "Magnetoencephalography— theory, instrumentation, and applications to noninvasive studies of the working human brain," *Reviews of Modern Physics*, vol. 65, no. 2, pp. 413–497, Apr. 1993.
3. D. B Geselowitz, "On the magnetic field generated outside an inhomogeneous volume conductor by internal volume currents," *IEEE Trans. Magn.*, vol. 6, pp. 346–347, 1970.
4. Jean-Claude Nédélec, *Acoustic and Electromagnetic Equations*, Springer Verlag, 2001.
5. J. Rahola and S. Tissari, "Iterative solution of dense linear systems arising from the electrostatic integral equation," *Phys. Med. Biol.*, , no. 47, pp. 961–975, 2002.
6. Jussi Rahola and Satu Tissari, "Iterative solution of dense linear systems arising from boundary element formulations of the biomagnetic inverse problem," Tech. Rep. TR/PA/98/40, CERFACS, 1998, Toulouse, France.
7. A. Steward Ferguson and Gerhard Stroink, "Factors affecting the accuracy of the boundary element method in the forward problem — I: Calculating surface potentials," *IEEE Trans. Biomed. Eng.*, vol. 44, no. 11, pp. 1139–1155, Nov. 1997.
8. Maureen Clerc, Renaud Keriven, Olivier Faugeras, Jan Kybic, and Theo Papadopoulo, "The fast multipole method for the direct E/MEG problem," in *Proceedings of ISBI*, Washington, D.C., July 2002, IEEE, NIH.
9. D. B. Geselowitz, "On bioelectric potentials in an homogeneous volume conductor," *Biophysics Journal*, vol. 7, pp. 1–11, 1967.
10. Jan Kybic, Maureen Clerc, Toufic Abboud, Olivier Faugeras, Renaud Keriven, and Théo Papadopoulo, "Integral formulations for the eeg problem," Tech. Rep. 4735, INRIA, Feb. 2003.
11. L. J. Gray and Glaucio H. Paulino, "Symmetric Galerkin boundary integral formulation for interface and multi-zone problems," *Internat. J. Numer. Methods Eng.*, vol. 40, no. 16, pp. 3085–3103, 1997.
12. J. B. Layton, S. Ganguly, C. Balakrishna, and J. H. Kane, "A symmetric Galerkin multi-zone boundary element formulation," *Internat. J. Numer. Methods Eng.*, vol. 40, no. 16, pp. 2913–2931, 1997.
13. T. F. Chan, "Deflated decomposition solution of nearly singular systems," *SIAM J. Numer. Anal.*, vol. 21, pp. 739–754, 1984.
14. Satu Tissari and Jussi Rahola, "Error analysis of a new Galerkin method to solve the forward problem in MEG and EEG using the boundary element method," Tech. Rep. TR/PA/98/39, CERFACS, 1998, Toulouse, France.

15. G. Fischer, B. Tilg, R. Modre, F. Hanser, B. Messnarz, and P. Wach, "On modeling the Wilson terminal in the Boundary and Finite Element Method," *IEEE Trans. Biomed. Eng.*, vol. 49, no. 3, pp. 217–224, Mar. 2002.
16. J. C. De Munck, "The potential distribution in a layered anisotropic spheroidal volume conductor," *J. Appl. Phys*, vol. 2, no. 64, pp. 464–470, July 1988.
17. Zhi Zhang, "A fast method to compute surface potentials generated by dipoles within multilayer anisotropic spheres," *Phys. Med. Biol.*, vol. 40, pp. 335–349, 1995.
18. John C. Mosher, Richard B. Leahy, and Paul S. Lewis, "EEG and MEG: Forward solutions for inverse methods," *IEEE Transactions on Biomedical Engineering*, vol. 46, no. 3, pp. 245–259, Mar. 1999.
19. M. S. Hämäläinen and J. Sarvas, "Realistic conductivity geometry model of the human head for interpretation of neuromagnetic data," *IEEE Trans. Biomed. Eng.*, vol. 36, no. 2, pp. 165–171, Feb. 1989.
20. M. Clerc, A. Dervieux, O. Faugeras, R. Keriven, J. Kybic, and T. Papadopoulo, "Comparison of BEM and FEM methods for the E/MEG problem," in *Proceedings of BIOMAG 2002*, Aug. 2002.
21. Richard Barret, Michael Berry, Tony F. Chan, James Demmel, June Donato, Jack Dongarra, Victor Eijkhout, Roldan Pozo, Charles Romine, and Henk van der Vonst, *Templates for the Solution of Linear Systems: Building Blocks for Iterative Methods*, SIAM, Philadelphia, 1994, Available from netlib.
22. S. Tissari and J. Rahola, "A precorrected-FFT method to accelerate the solution of the forward problem in MEG," in *Proceedings of BIOMAG*, 2002.
23. J. R. Phillips and J. K. White, "A precorrected-FFT method for electrostatic analysis of complicated 3-D structures," *IEEE Trans. CAD Int. Circ. Syst.*, vol. 16, no. 10, Oct. 1997.